

Assessment of soot particle vaporization effects during laser-induced incandescence with time-resolved light scattering

Gregory D. Yoder, Prasoon K. Diwakar, and David W. Hahn

Although laser-induced incandescence (LII) has been successfully used for soot volume fraction and particle size measurements, uncertainties remain regarding issues of soot vaporization leading to mass loss and morphological changes occurring in soot due to intense heating. Prompt LII detection schemes are often based on the assumption that the associated time scale is shorter than the time scale of soot vaporization or sublimation. The validity of such assumptions is the focus of the current study. Time-resolved light-scattering measurements were made in combination with LII measurements to quantify soot particle vaporization effects resulting from the LII laser pulse. The light-scattering measurements revealed a sharp decrease in total soot particle mass during the time course of the 25 ns full-width LII laser pulse for fluences in the range of 0.5 J/cm². Light-scattering theory was used to invert the scattering data, revealing $\approx 80\%$ – 90% reductions in the soot particle volume for LII fluences of 0.47 and 0.61 J/cm². In addition, the time-resolved scattering measurements show that the time scale of soot vaporization is completely confined to the LII laser pulse itself. Light scattering revealed no soot vaporization only for fluences of ~ 0.1 J/cm², which is consistent with recent work on low-fluence LII. Possible mechanisms for soot vaporization are discussed, notably for near-threshold fluences. © 2005 Optical Society of America
OCIS codes: 120.1740, 120.5820.

1. Introduction

Combustion-generated pollutants, notably soot, have become a cause of great concern in recent years, both with respect to the environment and human health. In response, stricter environmental standards and regulations dictate an urgent need to decrease emissions from combustion systems. Environmental protection agencies have generally focused on larger-sized particulate matter such as PM₁₀ (particles less than 10 μm in diameter) in the past, but recent U.S. regulations have started focusing on smaller particles (e.g., PM_{2.5}) because of increased health concerns caused by finer particulate matter.¹ Soot is generally accepted to contain carcinogenic components, and when inhaled the finer soot particles can have detrimental effects on people, even leading to premature deaths.^{2–4} In addition to environmental and health

considerations, soot formation also influences heat transfer, which may adversely affect the performance of practical combustors and increase their operating cost. Strategies for reduction of soot depend on the understanding of soot formation mechanics, which in turn may be aided by the capabilities of real-time monitoring of soot distributions, including reliable measurement of soot parameters such as particle size, number density, and soot volume fraction.

Various nonintrusive optical diagnostic techniques, including extinction and light-scattering techniques, have been applied to study soot. Using extinction (i.e., transmission measurements) techniques alone, soot volume fractions can be calculated in the Rayleigh regime, whereas using various combinations of extinction measurements, scattering measurements, dynamic light scattering, and transmission electron microscope (TEM) sampling, soot morphology and particle size information can be determined. Although useful, these traditional techniques are all characterized by certain limitations. For example, line-of-sight averaging by transmission measurements is impractical for use in turbulent flame conditions, and Rayleigh and Mie scattering are sensitive to particle shape and composition. Such limitations have led to the development of new soot

The authors are with the Department of Mechanical and Aerospace Engineering, University of Florida, Gainesville, Florida 32611-6300. D. W. Hahn's e-mail address is dwhahn@ufl.edu.

Received 13 September 2004; revised manuscript received 15 February 2005; accepted 18 February 2005.

0003-6935/05/204211-09\$15.00/0

© 2005 Optical Society of America

diagnostic techniques, including the method of laser-induced incandescence (LII), which holds promise as a reliable, sensitive, and easy to apply methodology for total soot measurements that combine high spatial and temporal resolution.

LII was first observed by Eckberth in 1977 when recording Raman measurements in a propane diffusion flame.⁵ In this early study, the LII phenomenon was considered a hindrance in Raman measurements, as it overwhelmed the Raman signals. In the following years, many research groups studied the phenomenon and developed models to relate LII signals to soot parameters such as soot volume fraction and particle size.^{6–8} Melton concluded that, at the moment of maximum soot temperature following laser heating, the LII signal, as detected in visible emission bands, is nominally proportional to soot volume fraction.⁶ Following these pioneering studies, LII became an extensively used laser diagnostic technique for soot. In the past two decades, many researchers have performed experimental and numerical studies to understand the basic principles of this technique,^{6,9–12} and LII has been successfully applied in a wide variety of systems. LII has been qualitatively and quantitatively used for both soot volume fraction and particle size diameter measurements in diesel engines, exhaust gases, premixed and diffusion flames, laminar and turbulent flames, and free-falling droplet flames, including both point measurements and two-dimensional imaging.^{9–11,13–17}

The basic principle in LII involves rapid heating of soot particles by use of intense laser pulses, whereby soot particles absorb laser energy and are consequently heated to the soot vaporization temperature of $\approx 4000\text{--}4500\text{ K}$.⁶ At these temperatures, which are significantly above the flame temperatures, blackbody radiation (i.e., incandescence) occurs, which is easily detected with photodetectors. Quantitative measurement of the soot volume fraction is performed by calibrating the LII system, typically by comparison with extinction measurements,¹⁸ gravimetric sampling analysis,¹⁹ or cavity ringdown measurements.^{20,21} LII signals persist for hundreds of nanoseconds, which is in contrast to many other laser-based techniques in which the analyte signal is coincident with the excitation source time scale (e.g., Raman and Rayleigh scattering). The temporal profile of the LII signal is useful, as the LII signal decay rate can be used to infer soot particle size.^{15,22} The temperature to which soot particles are heated depends on various competing processes.⁶ Following laser heating, energy is lost from the soot by soot vaporization, as well as convection and radiation heat transfer. Recently mechanisms for oxidation, melting and annealing of particles, and nonthermal desorption terms have also been included in LII models to better understand this complex process.²³

In general, various assumptions are involved in the treatment of the LII signal as proportional to the total soot volume fraction (f_v), notably the assumption that only negligible soot mass is lost due to vaporization. Various studies have reported good agreement

between f_v measurements based on the LII method and other techniques, but questions still remain concerning the role of vaporization and mass loss during LII and the implications on overall accuracy.

The laser fluence (pulse energy per area) is perhaps the most important LII parameter, and various studies have been performed to elucidate the effects of laser fluence. The laser fluence effect on the time-integrated LII signal depends on the spatial profile of the laser beam. It has been observed that, for a Gaussian spatial beam profile, the integrated LII signal increases as the fluence increases and then reaches a near-constant plateau region.^{10,24–26} For non-Gaussian profiles, different signal versus fluence curves are obtained. For example, for a top-hat profile a distinct maximum is obtained, and then the signal decreases as the fluence is further increased. In practice, generally the plateau region of the fluence curve as obtained by a Gaussian beam with unconstrained optics has been used by researchers for making qualitative measurements, as it minimizes any need for signal correction because of laser fluctuations or beam attenuation across the flame, provided that the fluence is well beyond the threshold fluence level for vaporization.²⁴ With Gaussian beams, however, caution must be noted with regard to fluences falling below the vaporization threshold in the wings of the Gaussian profile. This threshold fluence has been observed by many researchers to be $\approx 0.2\text{ J/cm}^2$. In this plateau region, the LII signal is assumed to be independent of fluence with minimal change in particle size taking place due to vaporization effects. But, as suggested by many researchers, this plateau region seems to be an artifact produced by two competing processes: an increase in the number of particles above the incandescence threshold in the beam profile wings, thereby leading to a larger probe volume, and a decrease in the LII signal due to an enhanced rate of soot vaporization with increasing laser fluence.^{25,27}

Studies have also been done to understand the effect of laser heating on the morphology of soot particles. In one such study, Vander Wal *et al.* showed that laser heating by a 1064 nm excitation wavelength causes graphitization and mass rearrangements for lower fluences and mass loss through vaporization at fluences above 0.5 J/cm^2 , coupled with a decrease in LII signal on a time scale of 100 ns.²⁸ Vander Wal *et al.* suggested use of laser fluence below the vaporization threshold to avoid any morphological changes in soot, especially when determining the particle size, and thereby promoting accuracy in LII measurements. For 532 nm laser excitation, Dasch reported a fluence of 0.23 J/cm^2 as the threshold for soot vaporization effects.^{7,8} Michelsen *et al.* reported a similar threshold value of 0.2 J/cm^2 for time-resolved LII experiments.²⁹ To avoid the many uncertainties in soot characterization by LII due to soot vaporization, as enumerated above, a low-fluence LII model has been proposed, and numerical and experimental studies have been performed recently.^{30,31}

In practical implementations, LII signals have been generally obtained by time averaging the instantaneous LII signal, with three detection techniques used: (i) prompt detection in which signals are averaged for $\approx 20\text{--}100$ ns coincident with the laser pulse; (ii) delayed detection technique in which the signal collection is delayed somewhat, generally 30–50 ns, after the laser pulse³²; and (iii) more recently low-fluence LII to completely avoid vaporization issues.^{30,31} Prompt LII detection has been generally preferred as a means to reduce effects of soot particle vaporization, based on the assumption that the measurement time scale is less than the time scale of significant soot vaporization. Prompt signals are also strong and have been demonstrated to be less sensitive to particle size effects. Delayed detection has the advantage of eliminating many spurious signals (e.g., fluorescence, photofragmentation), but also tends to promote signal bias toward larger soot particles. Mewes and Seitzman have shown that the error in soot volume fraction measurements due to particle size variation is less in prompt detection than delayed detection but still the error can reach up to 10%–25%.⁹ Mass loss of soot particles during the laser pulse, thereby reducing the particle size, can cause significant error in soot volume fraction measurement. Recently, Witze *et al.* proposed an instantaneous value analysis for LII signals to minimize the effect of reduced LII signals at higher fluences due to mass loss.²⁷ In aggregate, the above studies demonstrate the need for a better understanding of the roles of soot particle vaporization or sublimation, notably the vaporization time scale, in the context of LII. The primary goal of this study is to further elucidate the temporal nature of the soot vaporization phenomenon in the context of LII.

2. Experimental Methods

A propane diffusion flame was used for all experiments. The burner was constructed from two stainless-steel tubes, with an inner fuel tube diameter of 1.6 mm and an outer oxygen tube diameter of 7.1 mm. The propane flow was controlled by a precision-drilled ruby orifice (100 μm), which maintained a constant propane flow rate of 0.31 liters per minute (LPM). The annular flow of oxygen was maintained by a gas flow controller at a rate of 1.82 LPM. In addition, a perforated annular disk provided an outer shroud flow of nitrogen at 1 LPM, which enabled precise control over the fuel stoichiometry and was found to aid in flame stability. The fuel equivalence ratio is equal to 0.87, based on the propane and oxygen flow rates. Finally, a stainless-steel mesh flame holder was positioned 4 cm above the burner to provide additional flame stability.

A two-laser setup was used for all experiments, as shown in Fig. 1. A Q-switched 1064-nm Nd:YAG laser (13 ns FWHM) was used for LII. A Q-switched frequency-doubled 532 nm Nd:YAG laser (5 ns FWHM) was used for the light-scattering measurements. The 1064 nm laser light was focused on the center of the burner axis using a 500 nm focal-length

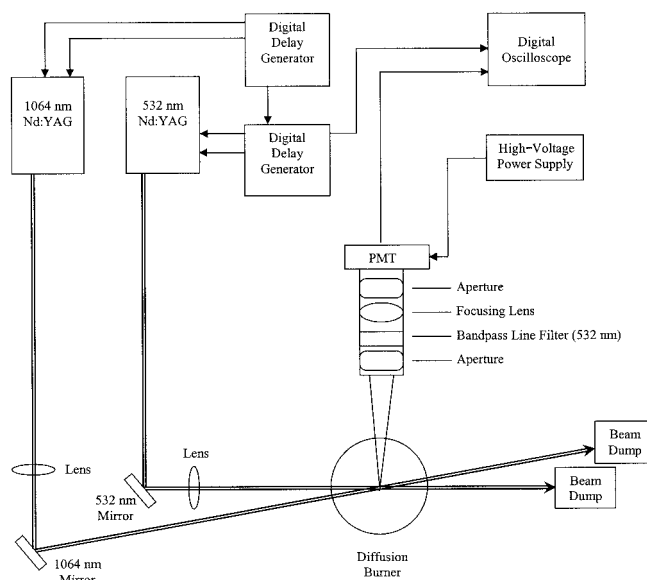


Fig. 1. Schematic of the experimental setup for time-resolved light scattering and LII measurements.

lens. The 1064 nm LII laser beam was analyzed using a beam profiler (Coherent Technologies) and is characterized by an 86.5% Gaussian fit ($1/e$ squared). Prior to focusing, the LII laser beam was passed through an aperture such that 90% of the laser-pulse energy was transmitted, which corresponds to a full beam width equal to 1.4 times the FWHM beam diameter based on the measured Gaussian fit. The 532 nm laser light was likewise focused to the center of the burner using a 250 mm focal-length lens. The 532 nm beam also had a Gaussian spatial beam profile, but was not characterized. The two laser beams were directed such that the beams crossed at their focal spots at a point on the central axis of the burner. The resulting focal spot of the 1064 nm beam was approximately four times the diameter of the 532 nm focal spot, and the 532 nm beam was centered in the middle of the 1064 nm beam. The optical configuration was designed to maximize the sensitivity of the scattering probe laser (i.e., 532 nm beam) to scattering particles within the LII probe volume (i.e., 1064 nm beam).

Both the LII signals and the light-scattering signals were collected at an angle of 90 deg with respect to the 532 nm light-scattering beam, as shown in Fig. 1. A 100 mm focal-length lens was used to image the focal volume onto a photomultiplier tube (PMT) with unity magnification. Apertures were placed on both ends of a 100 mm length lens tube to ensure high spatial resolution and to minimize stray light. The effective focal volume was 1.1 mm^3 , with an effective spatial resolution of 1.4 mm. A 532 nm interference filter (10 nm FWHM) was placed after the first aperture for all experiments. This enabled light-scattering measurements from the 532 nm laser, as well as LII measurements about a 532 nm bandwidth using the 1064 nm laser alone, without changing the experimental setup in any manner. C_2 emission

bands or Swan bands may be present at 473, 516, and 573 nm, and C_3 bands occur in 400–500 nm range. Although other emission bands may provide a more optimal LII signal (see Refs. 16, 18, 19, 26, and 29, for examples), use of the 532 nm interference filter as implemented in the current study effectively eliminated any possible interference from C_2 and C_3 emissions.²⁴

To effectively eliminate jitter between the two laser pulses, the flash lamp and Q switch of both lasers were externally controlled using a pair of digital delay generators with subnanosecond resolution. The first delay generator was internally triggered at a repetition rate of 5 Hz and was used to trigger the flash lamp and Q switch of the 1064 nm LII laser, as well as to trigger the second delay generator. The second delay generator then triggered the flash lamp and Q switch of the 532 nm scattering laser, as well as a digital oscilloscope (500 MHz, 4 gigasamples/s). A fast phototube (200 ps rise time) was used to determine relative timing between the two lasers. The time delay between the flash lamp and Q switch was optimized and held constant for both lasers. Timing between the two lasers was controlled by adjusting the delay between the flash-lamp triggers of the two lasers. As implemented, the jitter between the two laser pulses (peak to peak) was approximately 1 ns.

For both the light-scattering experiments and the LII experiments, signal linearity of the PMT was maintained by adjusting the PMT high voltage (staying within the optimal range) and using neutral-density (ND) filters in front of the outer aperture of the signal collection optics. For the signal linearity test of the PMT, a ND filter with a known attenuation factor of 2 was inserted or removed, and the expected factor of 2 change in signal was verified. Because PMTs are easily saturated with nanosecond laser pulse widths such as realized with prompt light scattering, signal linearity tests were performed prior to all measurements.

To assess the overall agglomerate soot particle size, soot samples were collected directly on coated copper TEM grids using thermophoretic sampling. For this procedure, the TEM grids were mounted to a sample holder and manually passed rapidly through the flame at the same height as the laser beams. The total residence time for thermophoretic sampling was less than ≈ 1 s, which was found to keep the grid coatings intact. Digital TEM micrographs were recorded, and an average soot particle size was determined by manually measuring the major and minor axis lengths of a number of soot agglomerates. In addition, the primary particles were discernable, and an average measure of the primary particle size was made.

3. Results and Discussion

To establish the relevant time scale of the LII signal, LII measurements were recorded using the 1064 nm laser in the absence of the 532 nm light-scattering laser. The 532 nm line filter was retained; hence the LII signal corresponds to a nominally 10 nm band-

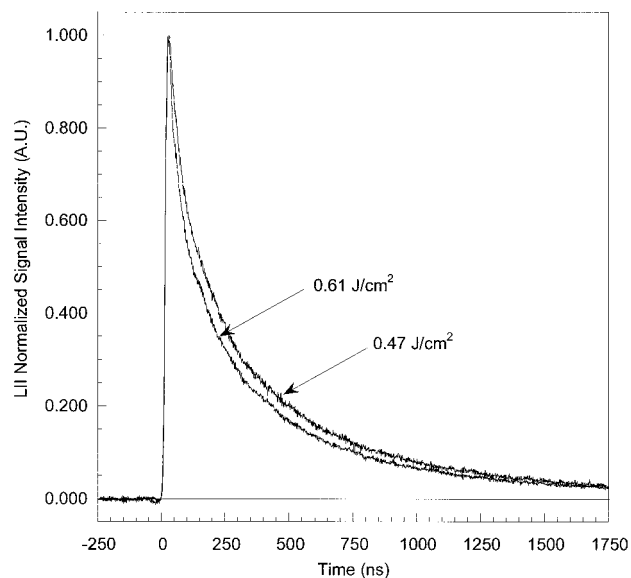


Fig. 2. Normalized LII signal as a function of time for laser fluences at 0.61 and 0.47 J/cm^2 . The signals are normalized to their maximum value, and the position of the incident laser pulse corresponds to zero.

width centered at 532 nm as discussed above. LII signals were recorded for laser fluences of 0.61 and 0.47 J/cm^2 , with the fluence based on the total laser-pulse energy and the measured laser spot size. The laser spot size was ≈ 1.4 mm, as measured by ablating ink from a glass microscope slide positioned at the beam focal spot. The ink ablation was found to produce a constant laser spot size over the range of laser-pulse energies; hence this value was taken as representative of the full beam width, noting the above comments with regard to the Gaussian fit.

For each LII measurement, the baseline signal (recorded with flame only) was subtracted from the recorded LII signal to establish a baseline of zero. This was done with the laser firing but with the laser shutter closed, which enabled subtraction of the electromagnetic noise originating from the laser Q switch. The flame-only signal was on average 8% of the LII signal, with a maximum of 13% and a minimum of 4% over all experiments. Each experiment was repeated a minimum of 12 times, and the baseline-corrected LII signal profiles were ensemble averaged to provide a final representative profile for each fluence. The resulting LII signals are presented in Fig. 2 corresponding to fluences of 0.61 and 0.47 J/cm^2 . As the focus of the current study was not an analysis of absolute LII signals, which have been well documented in Refs. 10, 24–27, the LII signals are presented normalized to their maximum values.

Figure 2 LII profiles reveal a rapid rise in signal that is temporally coincident with the incident laser pulse, followed by a monotonic decay over a time course of ≈ 1500 ns. The exact nature of the time-dependent LII signal with respect to the incident laser pulse is examined in detail in Subsection 3.A. In

general, the distinct signal rise is indicative of rapid laser heating of soot within the LII probe volume, whereas the steady decay following the end of the laser pulse is indicative of particle cooling due to heat transfer from the soot. The high gain and excellent linearity of the PMT enabled capture of the full decay range of the LII signal, which is consistent with reported LII particle temperature decay profiles, albeit at much lower laser fluences.³⁰ The role of soot vaporization is discussed in detail in Subsection 3.B. As expected within the region of laser fluences associated with vaporization or sublimation, the rate of decay of the LII signal increases with increasing laser fluence, presumably owing to the increased surface-to-volume ratio as the particles undergo a greater reduction in size owing to loss of particle mass.²⁹

A. Time-Resolved Light-Scattering and LII Measurements

The primary objective of the current study is to quantify the effects of soot particle vaporization during LII. We accomplished this using the 532 nm laser as a light-scattering probe. For discussion purposes, the 1064 nm laser used for the LII will be referred to as the LII laser, whereas the 532 nm laser used for light scattering will be referred to as the LS laser. For the light-scattering measurements, additional ND filters were added, with the result being that the contribution of the laser-induced incandescent signal from the LII laser was negligible. This was verified by the absence of any measurable signal for the LII laser alone with the ND filters in place. To eliminate any minimal contribution from the LII laser operation, mainly electromagnetic interference, baseline measurements were taken before and after the scattering measurements. These two baseline measurements (lasers operating, beams blocked) were averaged and then subtracted from the scattering signal, and the resulting integrated peak area was then calculated corresponding to the temporal width of the scattering laser pulse.

As described above, the LS laser was moved in time relative to the LII laser by use of the digital delay generator. For all experiments, the delay was initially adjusted such that the peak of the LS laser pulse was positioned 24 ns before the peak of the LII laser pulse, as shown in Fig. 3. Scattering data were then recorded at this delay, which provided a measure of the soot particle size prior to any possible soot particle vaporization, hence a scattering baseline. The delay was then adjusted to move the LS laser forward in time using 2 ns increments until the LS laser was positioned 20 ns after the LII laser pulse. The LS laser was then delayed further in time using larger increments up to a final delay of 132 ns beyond the LII laser pulse. For each delay, light-scattering measurements were recorded by averaging 500 laser pulses. These measurements were recorded for a minimum of 12 flame runs, with the final scattering data (scattering signal versus delay time) averaged to produce a representative time history of the light-scattering measurements. The light-scattering measurements were recorded for the same fluences used

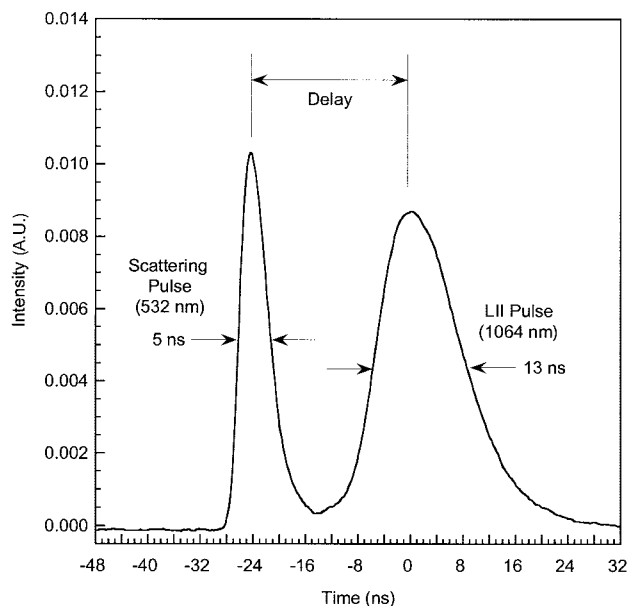


Fig. 3. Waveforms of the 532 nm LS laser pulse and the 1064 nm LII laser pulse showing the definition of the relative delay time. The relative intensity of the two waveforms is arbitrary.

for the Fig. 2 measurements, namely, fluences of 0.61 and 0.47 J/cm².

The light-scattering signals are presented in Fig. 4 as a function of delay time with respect to the LII laser pulse. For reference, the LII laser-pulse waveform is included in Fig. 4. While the scattering signal will be further quantified using Mie-scattering theory, several key features are observed with respect to the raw scattering signals in Fig. 4. Specifically, the rapid decrease in scattering signal is temporally co-

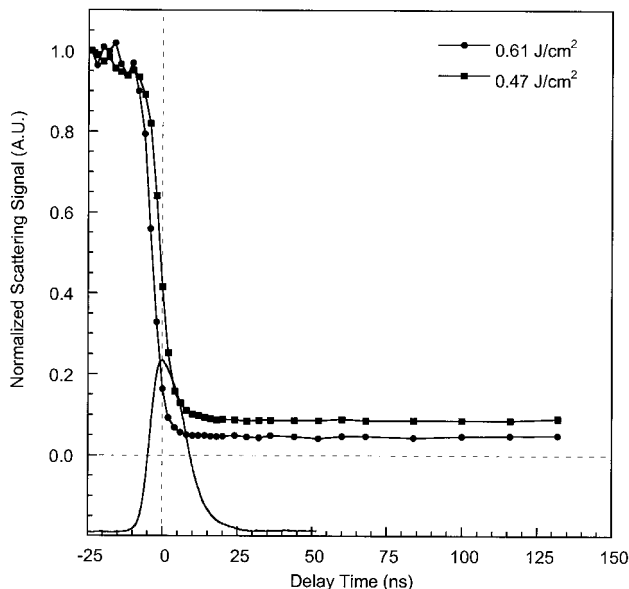


Fig. 4. Normalized light-scattering signal as a function of delay time between the scattering laser pulse and the LII laser pulse for LII laser fluences of 0.61 and 0.47 J/cm². The LII laser-pulse waveform is included as a reference.

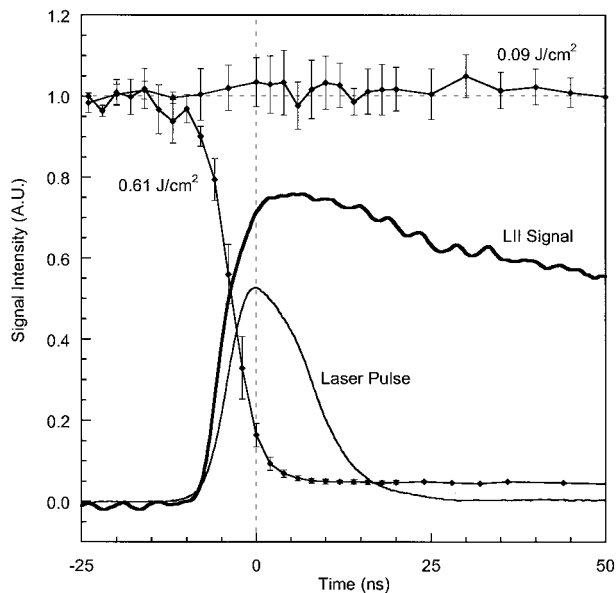


Fig. 5. Normalized light-scattering signal as a function of delay time between the scattering laser pulse and the LII laser pulse for LII laser fluences of 0.61 and 0.09 J/cm² and the LII signal as a function of time for a laser fluence at 0.61 J/cm². The light-scattering signals are labeled with the corresponding LII laser fluence and contain error bars equal to 1 standard deviation. The LII laser-pulse waveform (labeled as Laser Pulse) is included as a reference.

incident with the LII laser pulse, the majority of the decrease occurs prior to the peak of the LII pulse waveform, and the reduction in scattering signal abruptly flattens out with the end of the LII laser pulse. As expected for laser-induced soot particle vaporization, the decrease in light-scattering signal is enhanced with an increase in the fluence of the LII laser.

To gain additional insight into the temporal behavior of the light-scattering signal and the LII signal, the two data sets are superimposed in Fig. 5 for the LII laser fluence of 0.61 J/cm². The combination of LII data and light-scattering data clearly illustrates the comparable time scale of the laser heating (by the LII signal) and laser-induced soot vaporization (by the light-scattering signal). Previously, Witze *et al.* demonstrated in their experiments that the initiation of soot vaporization was coincident with the time scale of the LII laser pulse, although the temporal range of their scattering data was bound to the LII laser-pulse duration.²⁷ In the current study, the data clearly support the conclusion that the time scale of soot vaporization is not only coincident with the LII laser pulse for a Gaussian profile, but is actually confined entirely to the laser pulse, with the majority of vaporization occurring within the first half of the LII laser waveform. The implications on traditional LII approaches are twofold: First, use of prompt LII detection schemes in an effort to minimize soot vaporization processes is not well founded, and second use of delayed LII detection does isolate a temporal region of essentially constant soot particle volume

during the cooling process, although the isolated soot volume is necessarily reduced from the original soot volume for incident laser fluences above the vaporization threshold (i.e., ~ 0.1 J/cm²).

Careful examination of the curvature of the LII signal and the light-scattering signal during the first half of the LII laser waveform allows additional speculation as to the role of the laser-soot particle interaction processes. A discernable change in slope is observed in the LII signal profile approximately one fourth into the laser pulse; specifically the slope becomes less steep by a factor of approximately 3. It is noted here that the full width of the light-scattering probe laser was ≈ 12 ns; hence one must keep in mind the overall temporal resolution. Nonetheless, if one considers that the soot particles are heating throughout the entire first half of the LII laser pulse, thereby steadily increasing their emissive power, the break-point is interpreted to represent the onset of domination of soot vaporization or sublimation effects over soot particle heating. However, for such an effect to take place so early in the laser pulse where particle temperatures must be well below the maximum value (i.e., well before the LII signal maximum with concomitant vaporization) suggests that a laser ablation mechanism may be the key component of soot vaporization rather than soot particle sublimation following heating to the carbon melting point. This is consistent with the observed soot vaporization reported by Witze *et al.* at fluences well below the generally considered threshold for significant soot vaporization effects²⁷ and suggests that direct laser ablation and more traditional soot vaporization by laser heating are two competing effects. Throughout this paper, we have referred to loss of soot particle mass in general using the term vaporization, although a careful reading of the literature reveals at times clear demarcations among authors with regard to use of vaporization and sublimation. In the current context, the reported laser ablation effect may account for largest fraction of soot loss and may be consistent with the term sublimation by others to mean a direct conversion from the solid to gaseous state. Because laser ablation is not necessarily driven solely by temperature, the process of mass removal may be initiated at a critical photon flux occurring prior to the temporal peak of the laser-pulse width.

It is also useful to quantify conditions for the lack of any measurable soot vaporization by use of the light-scattering probe. A laser fluence value of 0.2 J/cm² has been remarkably robust as a threshold value for soot vaporization, as reported in a number of studies.^{7,8,18,27,29} Additional laser fluences were investigated in a similar manner as discussed above to assess the degree of soot vaporization for fluences near the range of 0.2 J/cm². For a fluence of 0.32 J/cm², the scattering signal exhibited a profile similar to the Fig. 4 data, although the final decrease in scattering signal was 29% with respect to the initial value. An incident fluence of 0.17 J/cm² resulted in a final scattering signal decrease of only 11%,

which is consistent with the published threshold values. It is important to note that Witze *et al.* reported a marked change in the LII signal that was attributed primarily to vaporization effects at a fluence of 0.2 J/cm², but also noted some mass loss at lower fluences,²⁷ which is consistent with our findings at a fluence of 0.17 J/cm². Finally, an incident laser fluence of 0.09 J/cm² resulted in no detectible soot particle reduction, as based on the light-scattering signal. For comparison with the measurements reported above, the scattering data for this fluence are also presented in Fig. 5.

B. Quantification of Soot Vaporization

As discussed above, the light-scattering measurements reveal a significant decrease in the soot particle scattering signal, as attributed to a combination of soot particle ablation and vaporization or sublimation processes. The measured scattering signal can be quantified to highlight the corresponding change in particle volume by using appropriate light-scattering theory in combination with the measured average soot particle size by the TEM analysis. The transmission electron microscopy results provided a measure of the size distribution of soot particles (i.e., soot agglomerates) corresponding to the relative flame position of the light-scattering measurements. The distribution was fit to a zeroth-order logarithmic distribution (ZOLD), which is an alternative form of the more general log-normal distribution function, as described by the function

$$p(a) = \frac{\exp(-\sigma_0^2/2)}{\sigma_0 a_m \sqrt{2\pi}} \exp\left[\frac{-(\ln a/a_m)^2}{2\sigma_0^2}\right], \quad (1)$$

in which a_m is the modal diameter and σ_0 is a dimensionless measure of width and skewness. These two parameters are readily related to the mean and true standard deviation as reported by Espenscheid and co-workers.³³ On the basis of the TEM data, the best fit was determined for a modal soot particle diameter of 75 nm and for a value of $\sigma_0 = 0.45$. The corresponding mean particle size and standard deviation are 100 and 48 nm, respectively. Also based on the TEM analysis, the mean primary soot particle size within the agglomerates was approximately 15 nm.

The measured scattering signal is a function of the collection optics, the solid angle of observation, and the detector efficiency, as well as the mean particle differential scattering cross section and the particle number density. The resulting equation for the scattering signal S_{vv} can be expressed as

$$S_{vv} = \beta C'_{vv} N, \quad (2)$$

where β is an experimental constant associated with the collection optics, the solid angle, and the detector efficiency; C'_{vv} is the mean differential scattering cross section (cm² sr⁻¹) for the soot particles; and N is the soot particle number density (cm⁻³). The sub-

scripts refer to the polarization state of the incident laser light and the scattered light, which were both vertically polarized with respect to the horizontal scattering plane. Taking the ratio of the scattering signal for any time versus the signal for the -24 ns delay (i.e., before any interaction with the LII laser pulse) will result in

$$C'_{vv}(t) = C'_{vv}(t = -24) \frac{S_{vv}(t)}{S_{vv}(t = -24)}. \quad (3)$$

Several assumptions are inherent in Eq. (3), including a constant value of β and that the diffusion time scale is long (of the order of microseconds) compared to the temporal range of scattering data (~100 ns), so that the particles can be considered frozen in time during the measurement, resulting in a constant number density.

Equation (3) allows the mean differential scattering cross section of the soot particles to be calculated as a function of time provided that the initial scattering cross section (i.e., delay of -24 ns) is known. Using full Mie theory for a polydispersion of scattering particles, we evaluated the initial scattering cross section using a modal diameter of 75 nm and a value of $\sigma_0 = 0.45$, as based on the TEM analysis; a complex refractive index of $m = 1.6 - 0.6i$ (Ref. 34); a scattering wavelength of 532 nm; and scattering angle of 90°. The soot modal diameter as a function of time was then calculated for each delay time by inverting the calculated cross sections using the same Mie theory and scattering parameters. For the LII laser fluences of 0.61 and 0.47 J/cm², the calculated soot modal diameters decreased from 75 nm to a final value of 39 and 43 nm, respectively.

The overall effect of the LII laser pulse on total soot particle volume fraction f_v can be inferred directly from the calculated modal diameters by integrating the particle size distribution

$$f_v = N \int_{a=0}^{\infty} \frac{\pi}{6} a^3 p(a) da. \quad (4)$$

In Eq. (4), $p(a)$ is the ZOLD particle size distribution and N is the particle number density. Assuming constant number density as discussed above, the modal diameters enable calculation of the normalized soot volume fraction as a function of delay with respect to the LII laser pulse. Using the first five delay points for normalization, the calculated soot particle volume is presented in Fig. 6 as a function of the delay time. The Fig. 6 data are characterized by a rapid decrease in soot volume, with the initial soot volume reduced by 86% and 81% for the fluences of 0.61 and 0.47 J/cm², respectively.

A few comments are noted with regard to the above analysis. Clearly the soot particles are not spherical in nature, as required for Mie analysis, but are characterized by an agglomerated structure of primary soot particles. In recent years, considerable research

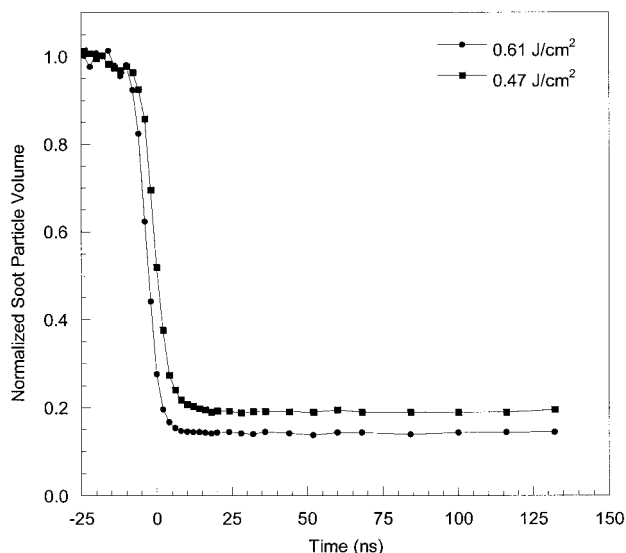


Fig. 6. Normalized soot particle volume as a function of delay time between the scattering laser pulse and the LII laser pulse for LII laser fluences of 0.61 and 0.09 J/cm^2 . The soot particle volume data correspond to the Fig. 4 scattering data after inversion with Mie-scattering theory.

has gone into modeling the light-scattering response of the agglomerated structures associated with soot. The most used theory is the so-called Rayleigh–Debye–Gans (RDG) theory, which is based on individual primary particles modeled as Rayleigh scatterers, while taking into account the fractal nature of the aggregates.^{35–37} A detailed treatment of the vaporization of soot particles in the context of RDG theory is beyond the scope of the present work, as the exact nature of the fractal characteristics in the context of aggregate vaporization is a complex problem. With these comments in mind, it is noted that Rayleigh and Mie scattering are still used to model soot scattering.^{38,39} The readers are therefore cautioned that the Fig. 6 analysis is presented to provide an estimate, notwithstanding the limitations of Mie theory, of the degree and temporal scale of soot particle mass loss.

As discussed above, such a significant loss of soot volume for even moderate LII fluences suggests that LII calibration must consider such vaporization effects. As concluded with the raw scattering data, the processes of soot volume loss are temporally confined entirely to the LII laser pulse, notably to the first half of the waveform.

4. Conclusions

The temporal evolution of the laser-induced incandescence process was analyzed in the context of soot particle vaporization using a time-resolved light-scattering probe. The current results clearly demonstrate that soot particle vaporization or sublimation, as characterized by a marked reduction in soot particle scattering size, is temporally coincident with the incident LII laser pulse, with no additional change in soot volume after the incident laser pulse. The often

used fluence threshold for soot vaporization, namely, $0.2 \text{ J}/\text{cm}^2$, is consistent with the results for minimal vaporization effects, although a factor of 2 below this value ($0.1 \text{ J}/\text{cm}^2$) was required to completely eliminate any soot vaporization, as verified by the sensitive light-scattering probe. Careful assessment of the temporal behavior of the LII signal and the light-scattering signal suggests that both laser ablation and traditional laser heating-induced vaporization may both be important processes, with the former concluded to play a key role at near-threshold fluences. An important implication of these findings is that laser-induced incandescence measurements must contend with soot volume loss effects in either prompt or delayed analysis schemes, except at very low fluences ($\sim 0.1 \text{ J}/\text{cm}^2$), which is consistent with recent efforts toward low-fluence LII.

This research was supported in part by the U.S. Office of Naval Research, Physical Sciences S&T Division, through contract N00014-0210838. The authors thank the reviewers for their detailed and thoughtful evaluations that elucidated several nuances of the LII technique.

References

1. U.S. Environmental Protection Agency, Office of Research and Development, "Air quality criteria for particulate matter (external review draft)," EPA/600/P-99/002 (U.S. Environmental Protection Agency, 1999).
2. F. Laden, L. M. Neas, D. W. Dockery, and J. Schwartz, "Association of fine particulate matter from different sources with daily mortality in six U.S. cities," *Environ. Health Perspect.* **108**, 941–947 (2000).
3. D. Liao, J. Creason, C. Shy, R. Williams, R. Watts, and R. Zweidinger, "Daily variation of particulate air pollution and poor cardiac autonomic control in the elderly," *Environ. Health Perspect.* **107**, 521–525 (1999).
4. J. M. Samet, F. Domnici, F. C. Curriero, I. Coursac, and S. L. Zeger, "Fine particulate air pollution and mortality in 20 U.S. cities, 1987–1994," *New Engl. J. Med.* **343**, 1742–1749 (2000).
5. A. C. Eckberth, "Effects of laser-modulated particulate incandescence on Raman scattering diagnostics," *J. Appl. Phys.* **48**, 4473–4479 (1977).
6. L. A. Melton, "Soot diagnostics based on laser heating," *Appl. Opt.* **23**, 2201–2208 (1984).
7. C. J. Dasch, "Continuous-wave probe laser investigation of laser vaporization of small soot particles in a flame," *Appl. Opt.* **23**, 2209–2215 (1984).
8. C. J. Dasch, "Spatially resolved soot-absorption measurements in flames using laser vaporization of particles," *Opt. Lett.* **9**, 214–216 (1984).
9. B. Mewes and J. M. Seitzman, "Soot volume fraction and particle size measurements with laser-induced incandescence," *Appl. Opt.* **36**, 709–717 (1997).
10. T. Ni, J. A. Pinson, S. Gupta, and R. J. Santoro, "Two-dimensional imaging of soot volume fraction by the use of laser-induced incandescence," *Appl. Opt.* **34**, 7083–7091 (1995).
11. N. P. Tait and D. A. Greenhalgh, "PLIF imaging of fuel fraction in practical devices and LII imaging of soot," *Ber. Bunsenges. Phys. Chem.* **97**, 1619–1625 (1993).
12. G. J. Smallwood, D. R. Snelling, F. Liu, and O. L. Gulder, "Clouds over soot evaporation: errors in modeling laser-induced incandescence of soot," *Trans. ASME* **123**, 814–818 (2001).

13. H. Zhao and N. Ladommatos, "Optical diagnostics for soot and temperature measurement in diesel engines," *Prog. Energy Combust. Sci.* **24**, 221–255 (1998).
14. D. L. Hofeldt, "Real-time soot concentration measurement technique for engine exhaust streams," SAE Tech. Paper 930079 (Society of Automotive Engineers, 1993).
15. S. Dankers and A. Leipertz, "Determination of primary particle size distributions from time-resolved laser-induced incandescence measurements," *Appl. Opt.* **43**, 3726–3731 (2004).
16. D. R. Snelling, G. J. Smallwood, R. A. Sawchuk, W. S. Neill, D. Gareau, W. L. Chippior, F. Liu, and O. L. Gulder, "Particulate matter measurements in a Diesel engine exhaust by laser-induced incandescence and the standard gravimetric procedure," SAE Tech. Paper 1999-01-3653 (Society of Automotive Engineers, 1999).
17. D. R. Snelling, G. J. Smallwood, R. A. Sawchuk, W. S. Neill, D. Gareau, D. J. Clavel, W. L. Chippior, F. Liu, and O. L. Gulder, "In-situ real-time characterization of particulate emissions from a Diesel engine exhaust by laser-induced incandescence," SAE Tech. Paper 2000-01-1994 (Society of Automotive Engineers, 2000).
18. B. Axelsson, R. Collin, and P.-E. Bengtsson, "Laser-induced incandescence for soot particle size and volume fraction measurements using on-line extinction calibration," *Appl. Phys. B* **72**, 367–372 (2001).
19. R. L. Vander Wal, Z. Zhuo, and Y. Choi, "Laser-induced incandescence calibration via gravimetric sampling," *Combust. Flame* **105**, 462–470 (1996).
20. R. L. Vander Wal and T. M. Ticich, "Cavity ringdown and laser-induced incandescence measurements of soot," *Appl. Opt.* **38**, 1444–1451 (1999).
21. C. S. Moreau, E. Therssen, X. Mercier, J. F. Pauwels, and P. Desgroux, "Two-color laser-induced incandescence and cavity ring-down spectroscopy for sensitive and quantitative imaging of soot and PAHs in flames," *Appl. Phys. B* **78**, 485–492 (2004).
22. R. L. Vander Wal, T. M. Ticich, and A. B. Stephens, "Can soot primary particle size be determined using laser-induced incandescence?" *Combust. Flame* **116**, 291–296 (1999).
23. H. A. Michelsen, "Understanding and predicting the temporal response of laser-induced incandescence from carbonaceous particles," *J. Chem. Phys.* **118**, 7012–7045 (2003).
24. R. L. Vander Wal and K. A. Jensen, "Laser-induced incandescence: detection issues," *Appl. Opt.* **35**, 6548–6559 (1996).
25. D. J. Bryce, N. Ladommatos, and H. Zhao, "Quantitative investigation of soot distribution by laser-induced incandescence," *Appl. Opt.* **39**, 5012–5022 (2000).
26. C. R. Shaddix and K. C. Smith, "Laser-induced incandescence measurements of soot production in steady and flickering methane, propane, and ethylene diffusion flames," *Combust. Flame* **107**, 418–452 (1996).
27. P. O. Witze, S. Hochgreb, D. Kayes, H. A. Michelsen, and C. R. Shaddix, "Time-resolved laser-induced incandescence and laser elastic-scattering measurements in a propane diffusion flame," *Appl. Opt.* **40**, 2443–2452 (2001).
28. R. L. Vander Wal, T. M. Ticich, and A. B. Stephens, "Optical and microscopy investigations of soot structure alterations by laser-induced incandescence," *Appl. Phys. B* **67**, 115–123 (1998).
29. H. A. Michelsen, P. O. Witze, D. Kayes, and S. Hochgreb, "Time-resolved laser-induced incandescence of soot: the influence of experimental factors and microphysical mechanisms," *Appl. Opt.* **42**, 5577–5590 (2003).
30. D. R. Snelling, F. Liu, G. J. Smallwood, and O. Gulder, "Determination of the soot absorption function and thermal accommodation coefficient using low-fluence LII in a laminar coflow ethylene diffusion flame," *Combust. Flame* **136**, 180–190 (2004).
31. F. Liu, G. J. Smallwood, and D. R. Snelling, "Effects of primary particle diameter and aggregate size distribution on the temperature of soot particles heated by pulsed lasers," *J. Quant. Spectrosc. Radiat. Transfer* **93**, 301–312 (2005).
32. F. Cignoli, S. Benecchi, and G. Zizak, "Time-delayed detection of laser-induced incandescence for the two-dimensional visualization of soot in flames," *Appl. Opt.* **33**, 5778–5782 (1994).
33. W. F. Espenscheid, M. Kerker, and E. Matijevic, "Logarithmic distribution functions for colloidal particles," *J. Phys. Chem.* **68**, 3093–3097 (1964).
34. K. C. Smyth and C. R. Shaddix, "Elusive history of $m = 1.57 - 0.56i$ for the refractive index of soot," *Combust. Flame* **107**, 314–320 (1996).
35. C. M. Sorensen, "Light scattering by fractal aggregates: a review," *Aerosol Sci. Technol.* **35**, 648–687 (2001).
36. S. S. Krishnan, K.-C. Lin, and G. M. Faeth, "Extinction and scattering properties of soot emitted from buoyant turbulent diffusion flames," *ASME J. Heat Transfer* **123**, 331–339 (2001).
37. H. W. Kim and M. Choi, "In situ line measurement of mean aggregate size and fractal dimension along the flame axis by planar laser light scattering," *Aerosol Sci.* **34**, 1633–1645 (2003).
38. C. R. Shaddix, J. E. Harrington, and K. C. Smyth, "Quantitative measurements of enhanced soot production in a flickering methane/air diffusion flame," *Combust. Flame* **99**, 723–732 (1994).
39. H. Bockhorn, H. Geitlinger, B. Jungfleisch, Th. Lehre, A. Schon, Th. Streibel, and R. Suntz, "Progress in characterization of soot formation by optical methods," *Phys. Chem. Chem. Phys.* **4**, 3780–3793 (2002).